

Two-dimensional ferromagnet/semiconductor transition metal dichalcogenide contacts: *p*-type Schottky barrier and spin-injection control

Li-Yong Gan, Qingyun Zhang, Yingchun Cheng,^{*} and Udo Schwingenschlöggl^{*}*PSE Division, KAUST, Thuwal 23955-6900, Kingdom of Saudi Arabia*

(Received 26 September 2013; published 18 December 2013)

We study the ferromagnet/semiconductor contacts formed by transition metal dichalcogenide monolayers, focusing on semiconducting MoS₂ and WS₂ and ferromagnetic VS₂. We investigate the degree of *p*-type doping and demonstrate tuning of the Schottky barrier height by vertical compressive pressure. An analytical model is presented for the barrier heights that accurately describes the numerical findings and is expected to be of general validity for all transition metal dichalcogenide metal/semiconductor contacts. Furthermore, magnetic proximity effects induce a 100% spin polarization at the Fermi level in the semiconductor where the spin splitting increases up to 0.70 eV for increasing pressure.

DOI: [10.1103/PhysRevB.88.235310](https://doi.org/10.1103/PhysRevB.88.235310)

PACS number(s): 73.22.-f, 73.21.Ac, 73.30.+y

I. INTRODUCTION

Two-dimensional (2D) materials exhibit unique properties, which often are distinctly different from their bulk counterparts, thus having created tremendous interest in synthesis and application.¹⁻³ In particular, the monolayers of semiconducting transition metal dichalcogenides (TMDCs), such as MoS₂ and WS₂, exhibit versatile electronic,⁴⁻⁸ optical,⁹⁻¹² mechanical,¹³⁻¹⁵ and chemical¹⁶⁻¹⁸ properties, offering opportunities beyond the more famous graphene and therefore opening up new fundamental as well as technological avenues for inorganic 2D materials in a range of fields, including electronic devices, catalysis, and energy storage.¹⁹ Semiconductor-to-metal transitions have been predicted for TMDC bilayers in external electric fields²⁰ and under vertical compressive pressure.²¹ In order to tune the electronic properties of semiconducting 2D TMDCs, hybrid systems have been put forward. Radisavljevic and co-workers²² have reported on few-layer 2D TMDC integrated electronic circuits that are able to perform digital logic operations. The MoS₂/graphene hybrid system has been reported to show a high electron conductivity and excellent electrochemical and thermoelectric performances.²³⁻²⁶ Therefore, combining TMDCs with other 2D layered materials is a viable and promising way to realize vertical heterostructures and hybrid all-2D devices.^{27,28}

Metal/semiconductor contacts play a key role in modern electronic and photonic devices, since the created Schottky barriers dominate the transport behavior.²⁹ It has been found that the barrier height in MoS₂ drastically depends on the electrodes.³⁰ More recently, a back gate voltage has been applied to manipulate the barrier height in MoS₂ field effective transistors contacted with cobalt electrodes.³¹ In addition, for potential spintronics applications, understanding the contacts with ferromagnetic substrates is crucial to realize efficient spin injection and enhance the spin polarization of the current across the interface.^{32,33} Introduction of transition metal atoms³⁴ and contacting with ferromagnetic substrates³¹ have been reported to yield spin injection and spin transport in monolayer MoS₂. 2D TMDCs constitute a large family of materials and possess the advantage that the electronic properties range from ferromagnets (such as VS₂ and NbS₂)³⁵⁻³⁸ to semiconductors,³⁹ opening the possibility of ferromagnet/semiconductor contacts for engineering all-2D electronic

devices and for realizing spin polarization.²⁸ In this context, we propose a class of ferromagnet/semiconductor contacts completely based on TMDC monolayers.

In the following, we investigate Schottky contacts in 2D TMDCs, focusing on the nonmagnetic semiconductors MoS₂ and WS₂ and the ferromagnet VS₂ as prototypes. We will argue that the degree of *p*-type doping and the corresponding Schottky barrier heights in MoS₂ and WS₂ can be controlled by vertical compressive pressure. A comprehensive picture is derived to understand the mechanism of the pressure dependence. We will also argue that magnetic proximity effects⁴⁰⁻⁴² induce 100% spin polarization in MoS₂ and WS₂ at the Fermi level (E_F) in a wide pressure range. These findings pave the way for designing coherent dopant-free all-2D contacts for future spin transport applications.

II. COMPUTATIONAL METHODS

First-principles calculations are performed using the Vienna Ab Initio Simulation Package with the spin polarized Perdew, Burke, and Ernzerhof generalized gradient approximation functional. In each case we apply a vacuum slab of at least 29 Å thickness. A cutoff energy of 500 eV and a Γ -centered $30 \times 30 \times 1$ *k*-mesh are used. The geometry is optimized until all residual forces are less than 0.01 eV/Å. Because of the absence of strong bonding a damped van der Waals correction,^{43,44} which is a significant improvement with respect to the generalized gradient approximation (though dipole-dipole corrections are limited in precision), is adapted to model nonbonding forces. We note that the Schottky barrier is an intrinsic property of the interface and defined by the relative alignment of E_F of the metal and the valence-band maximum (VBM, *p*-type barrier height $\Phi_{B,p}$) or conduction-band minimum (CBM, *n*-type barrier height $\Phi_{B,n}$) of the semiconductor.

III. RESULTS AND DISCUSSION

VS₂ monolayers exist in two polymorphs, trigonal prismatic (*h*VS₂) and octahedral (*t*VS₂), with D_{3h} and D_{3d} point groups, respectively.³⁹ Monolayer VS₂ has the former structure at and below room temperature.⁴⁵ The properties obtained in our calculations for the two phases are

TABLE I. Total energy (E_{tot} , normalized), energy difference (ΔE) between spin degeneracy and polarization, in-plane lattice constant (a), V-S bond length (d_{V-S}), layer thickness (d_{S-S}), magnetic moment (M), and work function (Φ) in the trigonal prismatic (hVS_2) and octahedral (tVS_2) phases.

	E_{tot} (meV)	ΔE (meV)	a (Å)	d_{V-S} (Å)	d_{S-S} (Å)	M (μ_B)	Φ (eV)
hVS_2	0	48	3.174	2.362	2.981	1.00	5.87
tVS_2	27	12	3.174	2.349	2.940	0.48	5.41

summarized in Table I. The former is 27 meV more stable, with the energy difference between spin degeneracy and polarization four times that of the latter. The in-plane lattice constants are the same, whereas the V-S bonds are slightly longer in hVS_2 . The calculated band structures, see Fig. 1, indicate that both phases are metallic with magnetic moments of 1.00 μ_B and 0.48 μ_B per unit cell. In hVS_2 the magnetic moments of V and S are 1.02 and -0.05 μ_B , respectively, while the corresponding values in tVS_2 are 0.51 and -0.03 μ_B . The calculated work function of hVS_2 is 0.46 eV larger than that of tVS_2 . All these results agree well with previous experimental and theoretical studies.^{35,37,46}

The relaxed lattice constant of both MoS_2 and WS_2 is 3.181 Å, i.e., the lattice mismatch to VS_2 is tiny ($\sim 0.2\%$). Thus, the average value of 3.177 Å is adopted for all the hybrid systems. For the contact with trigonal prismatic hVS_2 two stacking modes are considered, namely AA and AB, in which the Mo or W atoms are on top of V and S, respectively. Correspondingly, the interfaces are labeled hVS_2/MoS_2 -AA, hVS_2/MoS_2 -AB, hVS_2/WS_2 -AA, and hVS_2/WS_2 -AB. For the contact with octahedral tVS_2 there are in total six configurations: The atop-I and II patterns have S above S(1) and Mo or W above V and S(2), respectively, the hcp-I and II patterns have S above V and Mo or W above S(1) and S(2), and the fcc-I and II patterns have S above S(2) and Mo or W above S(1) and V. The structures of the hVS_2/MoS_2 and tVS_2/MoS_2 interfaces are shown in Fig. 2(d). The binding energy of an interface is defined as $E_B = E_{IS} - E_M - E_V$, where E_{IS} , E_M , and E_V represent the total energies of the hybrid system, MoS_2 or WS_2 , and VS_2 , respectively. The obtained binding energies per interface metal atom as a function of the interface separation D between MoS_2 or WS_2 and VS_2 are shown in Figs. 2(a)–2(c).

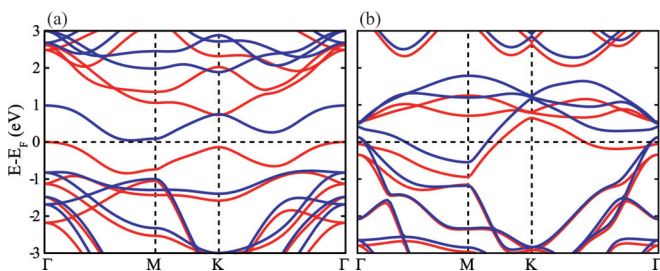


FIG. 1. (Color online) Spin polarized band structures of (a) hVS_2 and (b) tVS_2 . Red and blue lines correspond to the spin majority and minority bands, respectively.

We first focus on the bilayer systems with MoS_2 or WS_2 on VS_2 in the trigonal prismatic phase. As is shown in Figs. 2(a) and 2(b), the interaction between MoS_2 or WS_2 and VS_2 is similar to that in MoS_2/Ti_2CY_2 , -0.14 eV as compared to -0.13 eV at the respective equilibrium position.⁴⁷ Due to the larger S-S repulsion, the AA stacking is energetically less favorable in both hVS_2/MoS_2 and hVS_2/WS_2 . The equilibrium positions are the same in the two systems, 3.7 and 3.1 Å in the AA and AB stackings, respectively. For a separation larger than ~ 3.9 Å the AA and AB energy profiles overlap, indicating that the cases are degenerate with the interface formation still being exothermic. Figure 3 shows densities of states of MoS_2 , WS_2 , and VS_2 in hVS_2/MoS_2 -AA and hVS_2/WS_2 -AA at $D = 2.4$ Å and at the equilibrium positions to explore the electronic structure variations in the semiconductors upon the interface formation. It can be seen that the interface interaction modifies the electronic properties remarkably. At $D = 2.4$ Å distinct orbital overlaps between MoS_2 or WS_2 and VS_2 can be seen near E_F , suggesting strong hybridization. The induced states⁴⁸ near E_F suggest that the metallic character dominates the semiconducting natures of MoS_2 and WS_2 . The metallic features are different from those in semiconducting TMDCs bilayers, where they occur as upshift of the VBM at the Γ point and downshift of the CBM at the K point for decreasing interlayer separation.²¹ Additionally, evident spin polarization appears in both MoS_2 and WS_2 due to magnetic proximity effects.^{40–42} Because the effective S-S distance is much smaller in the AA stacking, a lower pressure threshold has been found for the semiconductor-to-metal transition in Ref. 21. It can be expected that similar metallic features in MoS_2 and WS_2 can be obtained in the AB stacking at high enough pressure. At the respective equilibrium positions in hVS_2/MoS_2 -AA and hVS_2/WS_2 -AA the density of states shows that both MoS_2 and WS_2 preserve their semiconducting characters with slightly smaller band gaps of 73 and 41 meV, respectively. Moreover, it can be seen from Figs. 3(b) and 3(d) that E_F is close to the VBM, indicating a strong p -type doping with barrier heights of 0.26 and 0.20 eV.

According to Figs. 2(a) and 2(b), it is much more likely to have AB stacking in hVS_2/MoS_2 and hVS_2/WS_2 interfaces for a separation less than 3.1 Å. Electronic band structures for AB stacking at $D = 2.4$ Å and at the equilibrium positions are given in Figs. 4(a) and 4(b). Due to the similarity between hVS_2/MoS_2 -AB and hVS_2/WS_2 -AB we only show the former case. At $D = 2.4$ Å the MoS_2 VBM at the Γ point is lifted higher than that at the K point due to the typical interface interaction,^{21,49} and the band gap is narrowed by 0.49 eV. Additionally, the VBM at the Γ point shows an evident spin splitting of 0.34 eV with one spin channel even crossing E_F , suggesting a shallow p -type doping. In the case of the equilibrium separation the VBM is still located at the Γ point, while the band-gap reduction (0.16 eV) and spin splitting (0.11 eV) are less pronounced. The VBM in both spin channels is located below E_F , giving rise to a p -type Schottky barrier of 0.20 eV. The trend of the band-gap variation and Γ point spin splitting for $D = 2.4$ to 3.1 Å in Fig. 4(d) shows that hVS_2/MoS_2 -AB and hVS_2/WS_2 -AB behave similarly: When the separation decreases the band gap decreases and the spin splitting increases monotonously. It can be deduced that further reduction of the interface separation will result in shallower

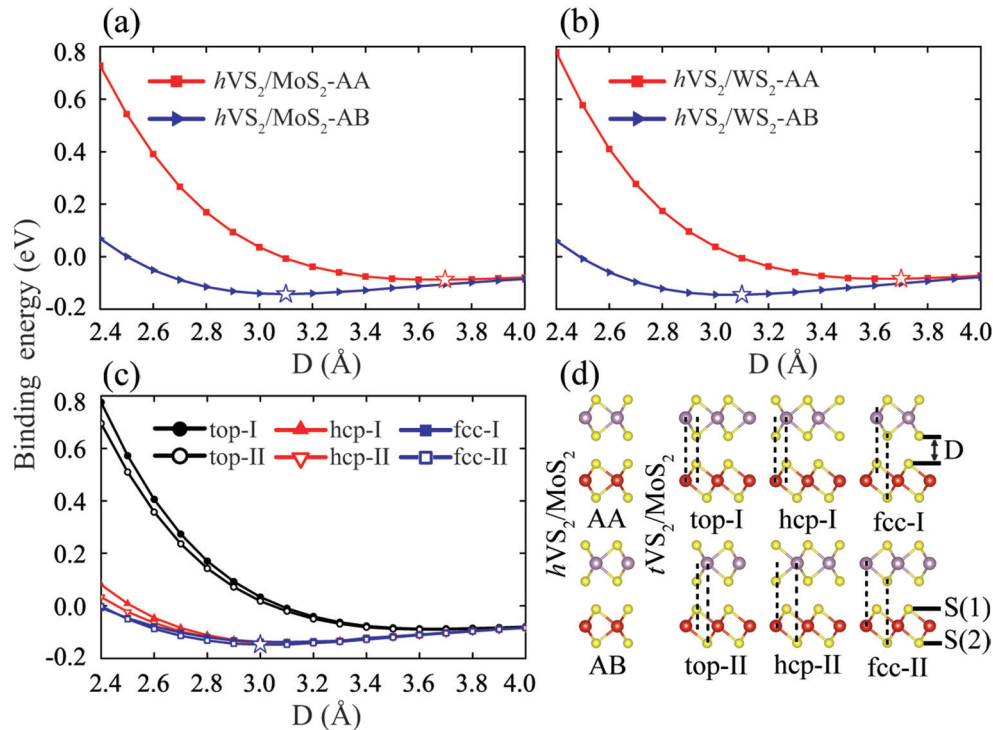


FIG. 2. (Color online) Binding energy per interface metal atom as a function of the interface separation (D) in (a) hVS_2/MoS_2 , (b) hVS_2/WS_2 , and (c) tVS_2/MoS_2 . The equilibrium positions are indicated by stars. (d) Side views of the nonequivalent configurations of hVS_2/MoS_2 and tVS_2/MoS_2 . Yellow, gray, and red balls represent S, Mo, and V atoms, respectively.

p -type doping and in an enhanced spin splitting in the two semiconductors.

We turn to the interfaces with VS_2 in the octahedral phase. As discussed above, MoS_2 and WS_2 in contact with hVS_2 show very similar results. Thus, we only consider the tVS_2/MoS_2 interface as an example. Figure 2(c) shows the binding energies as a function of the interface separation for the six configurations; see columns 2 to 4 in Fig. 2(d). According to the results, the six cases can be divided into two

groups, similar to hVS_2/MoS_2 : Arrangements with the S atom in MoS_2 on top of S(1) in tVS_2 , namely tVS_2/MoS_2 -top-I and II, are less stable and belong to the AA stacking class, while the other four types are similar to the AB stacking and are more likely to form. Specifically, the four cases are almost degenerate, with fcc-II being slightly more stable, suggesting that all can be fabricated. The band structure of the fcc-II

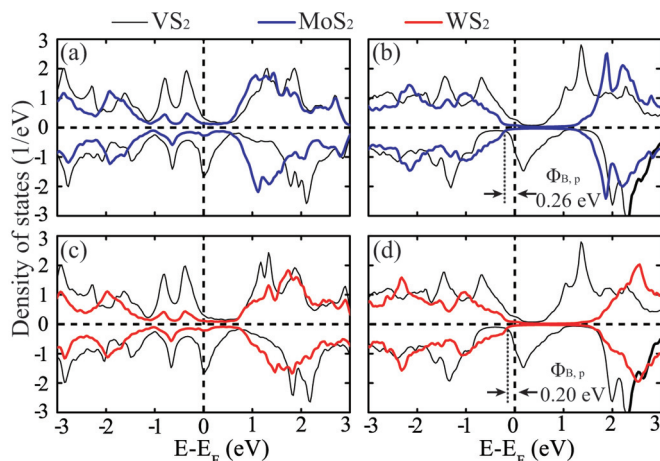


FIG. 3. (Color online) Spin polarized partial density of states for VS_2 , MoS_2 , and WS_2 in hVS_2/MoS_2 -AA and hVS_2/WS_2 -AA for (a), (c) an interface separation of 2.4 \AA and (b), (d) the equilibrium position. In (b) and (d) the p -type Schottky barrier heights ($\Phi_{B,p}$) are indicated.

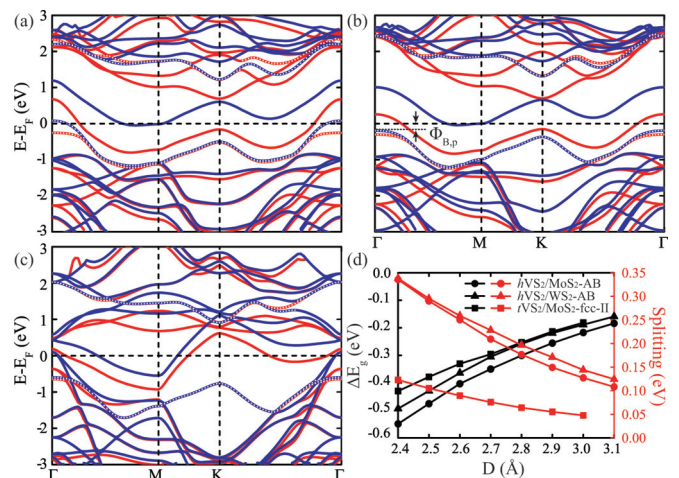


FIG. 4. (Color online) Spin polarized band structures of hVS_2/MoS_2 -AB for (a) $D = 2.4 \text{ \AA}$, (b) the equilibrium position, and (c) tVS_2/MoS_2 -fcc-II at the equilibrium position. The MoS_2 derived conduction and valence bands in the hybrid systems are indicated by white dotted curves. (d) Band-gap variation (black) and spin splitting at the Γ point (red) of MoS_2 and WS_2 as a function of the interface separation from $D = 2.4 \text{ \AA}$ to the respective equilibrium position.

configuration at the equilibrium separation of 3.0 Å is shown in Fig. 4(c) to investigate the electronic structure variations of MoS₂ in contact with *t*VS₂. The VBM of MoS₂ is located at the Γ point with the band gap narrowed by 0.18 eV and displays spin splitting. Moreover, E_F is located only 0.16 eV below the midgap (CBM+VBM)/2, suggesting rather weak *p*-type doping. The corresponding Schottky barrier height is calculated to be 0.60 eV. Figure 4(d) shows as a function of the interface separation the MoS₂ band-gap variation and VBM spin splitting in *t*VS₂/MoS₂-fcc-II. Similar to the trends in *h*VS₂/MoS₂-AB, the band gap increases and the spin splitting decreases monotonously as the separation increases, with the band-gap changes being comparable in *h*VS₂/MoS₂ and *h*VS₂/WS₂. However, a much smaller spin splitting is found in *t*VS₂/MoS₂-fcc-II due to the smaller magnetic moment of *t*VS₂.

It has been demonstrated above that different Schottky barrier heights are obtained by adjusting the interface separation in contact with both *h*VS₂ and *t*VS₂. In order to access the controllability of the barrier height in the experiment, the interface separations are next converted into vertical compressive pressures (P), which are calculated from the energy cost per unit area for reducing the separation,

$$P = \frac{E - E_0}{(D_0 - D)A}, \quad (1)$$

where E and E_0 are the total energies at interface separations of D and D_0 (equilibrium), and A is the area of the cell. Note that the pressure induced volume change is essentially due to the interface spacing, while only tiny shifts of the atomic positions are observed. The obtained barrier height as a function of P in *h*VS₂/MoS₂-AB (circles) and *t*VS₂/MoS₂-fcc-II (squares) is displayed in Fig. 6(b). At $P = 4.3$ ($D = 2.5$ Å) and 5.5 GPa ($D = 2.4$ Å) the VBM of MoS₂ at the Γ point is higher than E_F in *h*VS₂/MoS₂-AB [see Fig. 4(a)]. Thus, the Schottky barrier height is extended into the “negative” region for comparison. Obviously, a similar trend is found in the two systems: $\Phi_{B,p}$ decreases monotonously with increasing P . Also, the changes are reversible, i.e., the structures relax back to the equilibrium with larger $\Phi_{B,p}$ in the absence of pressure, making the systems potentially applicable in sensors. Pressure dependent *p*-type Schottky barrier heights, from another point of view, also constitute an effective strategy to control the degree of *p*-type doping in semiconducting TMDC monolayers. The present *p*-type doping together with the *n*-type doping found in MoS₂ on transition metal substrates^{30,31} opens access to *p-n* junctions.

In order to better understand the metal-semiconductor junctions, we address the plane-averaged charge density difference $\Delta\rho(z)$ to visualize the charge redistribution at the interface. The case of *h*VS₂/MoS₂-AB at the equilibrium separation is shown in Fig. 5(a); similar plots are found for the other studied systems. It can be seen that electrons are transferred from the semiconductor side to the interface and the VS₂ side, consistent with the results of *p*-type doping in MoS₂. The induced charge transfer, which is estimated by integrating $\Delta\rho(z)$, amounts to 0.019 $|e|$. Particularly, a charge accumulation can be seen around the V layer, yielding a smaller local magnetic moment with respect to pristine *h*VS₂ (0.92 versus 1.02 μ_B). Figure 5(b) shows the separation dependent charge transfer

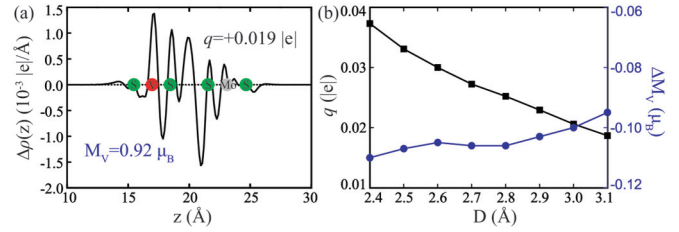


FIG. 5. (Color online) (a) Plane-averaged difference of the electron density, $\Delta\rho(z)$, for *h*VS₂/MoS₂-AB at the equilibrium position. The positions of the atoms are indicated, q is the charge transfer, and M_V is the magnetic moment of the V atom. (b) q (black) and M_V variation (ΔM_V , blue) as a function of the interface separation in *h*VS₂/MoS₂-AB.

and V magnetic moment. When the separation increases, both decrease gradually. This implies that the layer-layer interaction does not preclude charge transfer at the interface, similar to findings for MoS₂/Ti₂CY₂.⁴⁷ However, the charge transfer here is the opposite direction, so that an integration of MoS₂/VS₂ and MoS₂/Ti₂CY₂ would give rise to a coherent dopant-free all-2D *p-n* junction.^{28,50}

A schematic model is introduced in Fig. 6(a) to explain the effects on the *p*-type Schottky barrier height, which can be written as⁵¹

$$\Phi_{B,p} = I_{\text{MoS}_2} - \Phi_{\text{VS}_2} - \mu_{\text{IS}}, \quad (2)$$

where I_{MoS_2} and Φ_{VS_2} are the electronic ionization potential of MoS₂ and the work function of VS₂, respectively. At the contact of MoS₂ and VS₂ an interface dipole μ_{IS} occurs as a result of charge rearrangements. Its sign is negative, since the charge is transferred away from the semiconductor side. Additionally, due to the interaction between Γ point states,⁴⁹ the VMB of MoS₂ shifts upwards by Δ from its original position. Note that the semiconducting nature of MoS₂ (or WS₂) is preserved. The modification of the VS₂ work function is found to be tiny, i.e., $\Phi_{\text{VS}_2} \approx \Phi_{\text{VS}_2}^0$. As a consequence, Eq. (2) can be rewritten as

$$\begin{aligned} \Phi_{B,p} &= (I_{\text{MoS}_2}^0 - \Delta) - \Phi_{\text{VS}_2}^0 - \mu_{\text{IS}} \\ &= (I_{\text{MoS}_2}^0 - \Phi_{\text{VS}_2}^0) - \Delta - \mu_{\text{IS}}, \end{aligned} \quad (3)$$

where the superscript “0” denotes the pristine systems. Data obtained from Eq. (3) are shown by lines in Fig. 6(b) and reproduce the results of the band structure calculations very well. This fact suggests that three factors together determine the Schottky barrier height. The first is the intrinsic (and thus contact) difference between the electronic ionization potentials and work functions, respectively, of the pristine semiconductor and metal monolayers. The second is the MoS₂/VS₂ interface interaction, which leads to MoS₂ VBM upshifts. Note that, according to Ref. 47, even a large dipole shifts the energy levels only slightly. The last is the charge redistribution induced interface dipole. The interface barrier and MoS₂ VBM upshift as a function of the separation are shown in Figs. 6(c) and 6(d), respectively. It can be seen that the latter two factors are larger in *h*VS₂/MoS₂-AB, suggesting a stronger interaction and more pronounced charge transfer. The third factor depends less on D due to its long-range nature. The ionization potential of

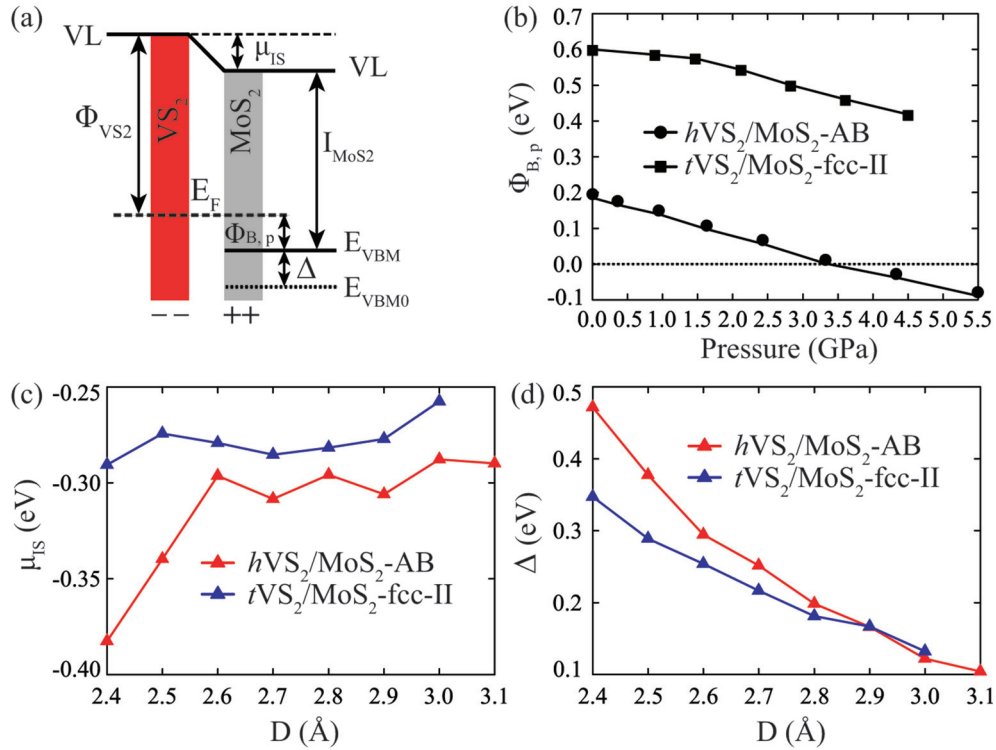


FIG. 6. (Color online) (a) Schematic diagram of the Schottky barrier formation. (b) Schottky barrier height as a function of the vertical compressive pressure in $hVS_2/\text{MoS}_2\text{-AB}$ (circles) and $tVS_2/\text{MoS}_2\text{-fcc-II}$ (squares). The lines represent the results obtained from Eq. (3). (c) Interface dipole (μ_{IS}) and (d) MoS_2 VBM upshift (Δ) as a function of D from 2.4 Å to the respective equilibrium positions.

pristine MoS_2 is 5.88 eV, giving the first contribution a value of 0.01 eV in $hVS_2/\text{MoS}_2\text{-AB}$. Accordingly, $\Phi_{B,p}$ is determined by the latter two contributions, where the second is larger than the third for pressure larger than 3.4 GPa, leading to negative barrier heights. In tVS_2/MoS_2 the first contribution (0.47 eV) is dominant and the latter two almost cancel out each other, thus resulting in higher barriers; see Fig. 6(b). By the similarity of this picture with TMDC/TMDC bilayers, the analytical model can be expected to be applicable to all TMDC metal/semiconductor contacts.

Understanding the spin injection into semiconducting 2D materials is important for spintronics applications. Figure 4(a) demonstrates 100% spin polarization in MoS_2 at E_F with one spin channel crossing E_F while the other stays below at $D = 2.4$ Å ($P = 5.5$ GPa) in $hVS_2/\text{MoS}_2\text{-AB}$. Similar results are obtained for $hVS_2/\text{WS}_2\text{-AB}$. The results imply that it is feasible to achieve 100% spin polarization in an appropriate pressure range. According to Fig. 6(b), the minimum pressure for which the VBM at the Γ point develops a spin splitting and one spin channel crosses E_F is around 3.4 GPa. The maximum pressure at which the metallic feature becomes dominant in MoS_2 , as is the case in $hVS_2/\text{MoS}_2\text{-AA}$ for $D = 2.4$ Å [see Fig. 3(a)], is calculated to be around 18 GPa. Additionally, when the pressure increases from 3.4 to 18 GPa the spin splitting becomes larger and finally a value of 0.70 eV is obtained. However, in tVS_2/MoS_2 , due to the large difference (0.47 eV) between the ionization potential of pristine MoS_2 and the work function of tVS_2 , the two spin channels at the VBM of MoS_2 in the hybrid system hardly will shift above E_F , making it unlikely to have the same result as in tVS_2/MoS_2 . Consequently, contacting MoS_2 with hVS_2 is a good

strategy to realize an efficient spin injection for spintronics applications.

IV. CONCLUSIONS

We have discussed the results of first-principles calculations for the prototypical VS_2/MoS_2 and VS_2/WS_2 contacts to explore the physics of metal/semiconductor contacts constructed of TMDC monolayers. The degree of p -type doping as well as the Schottky barrier height in MoS_2 and WS_2 upon interface formation can be readily tuned by vertical compressive pressure. In addition, an analytical model has been introduced to understand which quantities determine the barrier height and to which degree. An almost ideal accuracy of the model suggests that three factors play the key role: the difference between the electronic ionization potential of the semiconductor and the work function of the metal, the VBM upshift, and the interface dipole. Moreover, similarity with the interaction in TMDC/TMDC bilayer systems indicates that the model is of general validity for TMDC metal/semiconductor contacts.

As a consequence of magnetic proximity effects, 100% spin polarization at E_F is achieved in the MoS_2 layer in the pressure range from approximately 3.4 to 18 GPa. Within this range the spin splitting increases up to 0.70 eV. The obtained insights into 2D TMDC contacts are significant for designing all-2D metal/semiconductor contacts and also for further spin transport explorations.

ACKNOWLEDGMENT

This work was supported by a KAUST CRG grant and computational resources were provided by KAUST HPC.

*Author to whom correspondence should be addressed: yingchun.cheng@kaust.edu.sa; udo.schwingenschloegl@kaust.edu.sa

- ¹C. Lee, Q. Li, W. Kalb, X.-Z. Liu, H. Berger, R. W. Carpick, and J. Hone, *Science* **328**, 76 (2010).
- ²F. Schwierz, *Nat. Nanotechnol.* **5**, 487 (2010).
- ³L. Britnell, R. V. Gorbachev, R. Jalil, B. D. Belle, F. Schedin, A. Mishchenko, T. Georgiou, M. I. Katsnelson, L. Eaves, S. V. Morozov, N. M. R. Peres, J. Leist, A. K. Geim, K. S. Novoselov, and L. A. Ponomarenko, *Science* **335**, 947 (2012).
- ⁴B. Radisavljevic, A. Radenovic, J. Brivio, V. Giacometti, and A. Kis, *Nat. Nanotechnol.* **6**, 147 (2011).
- ⁵Z. Y. Zhu, Y. C. Cheng, and U. Schwingenschlögl, *Phys. Rev. B* **84**, 153402 (2011).
- ⁶D. Xiao, G.-B. Liu, W. Feng, X. Xu, and W. Yao, *Phys. Rev. Lett.* **108**, 196802 (2012).
- ⁷P. Johari and V. B. Shenoy, *ACS Nano* **6**, 5449 (2012).
- ⁸Y. Y. Hui, X. Liu, W. Jie, N. Y. Chan, J. Hao, Y.-T. Hsu, L.-J. Li, W. Guo, and S. P. Lau, *ACS Nano* **7**, 7126 (2013).
- ⁹K. F. Mak, C. Lee, J. Hone, J. Shan, and T. F. Heinz, *Phys. Rev. Lett.* **105**, 136805 (2010).
- ¹⁰Z. Yin, H. Li, H. Li, L. Jiang, Y. Shi, Y. Sun, G. Lu, Q. Zhang, X. Chen, and H. Zhang, *ACS Nano* **6**, 74 (2012).
- ¹¹K. F. Mak, K. He, C. Lee, G. H. Lee, J. Hone, T. F. Heinz, and J. Shan, *Nat. Mater.* **12**, 207 (2013).
- ¹²P. Johari and V. B. Shenoy, *ACS Nano* **5**, 5903 (2011).
- ¹³S. Bertolazzi, J. Brivio, and A. Kis, *ACS Nano* **5**, 9703 (2011).
- ¹⁴J. Pu, Y. Yomogida, K.-K. Liu, L.-J. Li, Y. Iwasa, and T. Takenobu, *Nano Lett.* **12**, 4013 (2012).
- ¹⁵A. Castellanos-Gomez, M. Poot, G. A. Steele, H. S. J. van der Zant, N. Agrait, and G. Rubio-Bollinger, *Adv. Mater.* **24**, 772 (2012).
- ¹⁶M. A. Lukowski, A. S. Daniel, F. Meng, A. Forticaux, L. Li, and S. Jin, *J. Am. Chem. Soc.* **135**, 10274 (2013).
- ¹⁷D. Voiry, H. Yamaguchi, J. Li, R. Silva, D. C. B. Alves, T. Fujita, M. Chen, T. Asefa, V. B. Shenoy, G. Eda, and M. Chhowalla, *Nat. Mater.* **12**, 850 (2013).
- ¹⁸X. Huang, Z. Zeng, S. Bao, M. Wang, X. Qi, Z. Fan, and H. Zhang, *Nat. Commun.* **4**, 1444 (2013).
- ¹⁹M. Chhowalla, H. S. Shin, G. Eda, L.-J. Li, K. P. Loh, and H. Zhang, *Nat. Chem.* **5**, 263 (2013).
- ²⁰A. Ramasubramaniam, D. Naveh, and E. Towe, *Phys. Rev. B* **84**, 205325 (2011).
- ²¹S. Bhattacharyya and A. K. Singh, *Phys. Rev. B* **86**, 075454 (2012).
- ²²B. Radisavljevic, M. B. Whitwick, and A. Kis, *ACS Nano* **5**, 9934 (2011).
- ²³K. Chang and W. Chen, *Chem. Commun.* **47**, 4252 (2011).
- ²⁴K. Chang and W. Chen, *ACS Nano* **5**, 4720 (2011).
- ²⁵Y. Li, H. Wang, L. Xie, Y. Liang, G. Hong, and H. Dai, *J. Am. Chem. Soc.* **133**, 7296 (2011).
- ²⁶W. Zhang, C.-P. Chuu, J.-K. Huang, C.-H. Chen, M.-L. Tsai, Y.-H. Chang, C.-T. Liang, J.-H. He, M.-Y. Chou, and L.-J. Li, [arXiv:1302.1230](https://arxiv.org/abs/1302.1230).
- ²⁷J. N. Coleman, M. Lotya, A. O'Neill, S. D. Bergin, P. J. King, U. Khan, K. Young, A. Gaucher, S. De, R. J. Smith, I. V. Shvets, S. K. Arora, G. Stanton, H.-Y. Kim, K. Lee, G. T. Kim, G. S. Duesberg, T. Hallam, J. J. Boland, J. J. Wang, J. F. Donegan, J. C. Grunlan, G. Moriarty, A. Shmeliov, R. J. Nicholls, J. M. Perkins, E. M. Grieveson, K. Theuwissen, D. W. McComb, P. D. Nellist, and V. Nicolosi, *Science* **331**, 568 (2011).
- ²⁸Q. H. Wang, K. Kalantar-Zadeh, A. Kis, J. N. Coleman, and M. S. Strano, *Nat. Nanotechnol.* **7**, 699 (2012).
- ²⁹I. Popov, G. Seifert, and D. Tománek, *Phys. Rev. Lett.* **108**, 156802 (2012).
- ³⁰W. Chen, E. J. G. Santos, W. Zhu, E. Kaxiras, and Z. Zhang, *Nano Lett.* **13**, 509 (2013).
- ³¹J.-R. Chen, P. M. Odenthal, A. G. Swartz, G. C. Floyd, H. Wen, K. Y. Luo, and R. K. Kawakami, *Nano Lett.* **13**, 3106 (2013).
- ³²E. I. Rashba, *Phys. Rev. B* **62**, R16267 (2000).
- ³³G. Schmidt, D. Ferrand, L. W. Molenkamp, A. T. Filip, and B. J. van Wees, *Phys. Rev. B* **62**, R4790 (2000).
- ³⁴Y. C. Cheng, Z. Y. Zhu, W. B. Mi, Z. B. Guo, and U. Schwingenschlögl, *Phys. Rev. B* **87**, 100401 (2013).
- ³⁵Y. Ma, Y. Dai, M. Guo, C. Niu, Y. Zhu, and B. Huang, *ACS Nano* **6**, 1695 (2012).
- ³⁶Y. Zhou, Z. Wang, P. Yang, X. Zu, L. Yang, X. Sun, and F. Gao, *ACS Nano* **6**, 9727 (2012).
- ³⁷J. Feng, X. Sun, C. Wu, L. Peng, C. Lin, S. Hu, J. Yang, and Y. Xie, *J. Am. Chem. Soc.* **133**, 17832 (2011).
- ³⁸K. Xu, P. Chen, X. Li, C. Wu, Y. Guo, J. Zhao, X. Wu, and Y. Xie, *Angew. Chem. Int. Ed.*, doi:10.1002/anie.201304337.
- ³⁹C. Ataca, H. Şahin, and S. Ciraci, *J. Phys. Chem. C* **116**, 8983 (2012).
- ⁴⁰H. Haugen, D. Huertas-Hernando, and A. Brataas, *Phys. Rev. B* **77**, 115406 (2008).
- ⁴¹D. Liu, Y. Hu, H. Guo, and X. F. Han, *Phys. Rev. B* **78**, 193307 (2008).
- ⁴²H. X. Yang, A. Hallal, D. Terrade, X. Waintal, S. Roche, and M. Chshiev, *Phys. Rev. Lett.* **110**, 046603 (2013).
- ⁴³T. Bucko, J. Hafner, S. Lebégue, and J. G. Ángyán, *J. Phys. Chem. A* **114**, 11814 (2010).
- ⁴⁴S. Grimme, *J. Comput. Chem.* **27**, 1787 (2006).
- ⁴⁵H. Zhang, L.-M. Liu, and W.-M. Lau, *J. Mater. Chem. A* **1**, 10821 (2013).
- ⁴⁶C. S. Rout, B.-H. Kim, X. Xu, J. Yang, H. Y. Jeong, D. Odkhuu, N. Park, J. Cho, and H. S. Shin, *J. Am. Chem. Soc.* **135**, 8720 (2013).
- ⁴⁷L.-Y. Gan, Y.-J. Zhao, D. Huang, and U. Schwingenschlögl, *Phys. Rev. B* **87**, 245307 (2013).
- ⁴⁸J. Tersoff, *Phys. Rev. Lett.* **52**, 465 (1984).
- ⁴⁹H.-P. Komsa and A. V. Krasheninnikov, *Phys. Rev. B* **88**, 085318 (2013).
- ⁵⁰G. Eda, T. Fujita, H. Yamaguchi, D. Voiry, M. Chen, and M. Chhowalla, *ACS Nano* **6**, 7311 (2012).
- ⁵¹R. T. Tung, *Phys. Rev. Lett.* **84**, 6078 (2000).